Biochimica et Biophysica Acta 1848 (2015) 942–950

Contents lists available at ScienceDirect

Biochimica et Biophysica Acta

journal homepage: www.elsevier.com/locate/bbamem

Relationships between membrane water molecules and Patman equilibration kinetics at temperatures far above the phosphatidylcholine melting point

Alexandra R. Vaughn, Thomas A. Bell, Elizabeth Gibbons, Caitlin Askew, Hannabeth Franchino, Kelsey Hirsche, Linea Kemsley, Stephanie Melchor, Emma Moulton, Morgan Schwab, Jennifer Nelson, John D. Bell *

Department of Physiology and Developmental Biology, Brigham Young University, Provo, Utah 84602, USA

ARTICLE INFO

Article history:
Received 27 October 2014
Received in revised form 18 December 2014
Accepted 24 December 2014
Available online 2 January 2015

Keywords:
Fluorescence
Patman
Laurdan
Kinetics
Membrane water
Liquid–Crystalline

ABSTRACT

The naphthalene-based fluorescent probes Patman and Laurdan detect bilayer polarity at the level of the phospholipid glycerol backbone. This polarity increases with temperature in the liquid–crystalline phase of phosphatidylcholines and was observed even 90 °C above the melting temperature. This study explores mechanisms associated with this phenomenon. Measurements of probe anisotropy and experiments conducted at 1 M NaCl or KCl (to reduce water permittivity) revealed that this effect represents interactions of water molecules with the probes without proportional increases in probe mobility. Furthermore, comparison of emission spectra to Monte Carlo simulations indicated that the increased polarity represents elevation in probe access to water molecules rather than increased mobility of relevant bilayer waters. Equilibration of these probes with the membrane involves at least two steps which were distinguished by the membrane microenvironment reported by the probe. The difference in those microenvironments also changed with temperature in the liquid–crystalline phase in that the equilibrium state was less polar than the initial environment detected by Patman at temperatures near the melting point, more polar at higher temperatures, and again less polar as temperature was raised further. Laurdan also displayed this level of complexity during equilibration, although the relationship to temperature differed quantitatively from that experienced by Patman. This kinetic approach provides a novel way to study in molecular detail basic principles of what happens to the membrane environment around an individual amphipathic molecule as it penetrates the bilayer. Moreover, it provides evidence of unexpected and interesting membrane behaviors far from the phase transition.

© 2014 Elsevier B.V. All rights reserved.

1. Introduction

Naphthalene derivatives (e.g. Prodan, Laurdan, and Patman) have been available for over thirty years as probes of membrane structure and dynamics [1–3]. Their utility stems from their strong sensitivity to general solvent effects. Specifically, their emission spectra shift by about 60 nm toward longer wavelength when water molecules present in the head-group region of the bilayer are able to align with the excited-state dipole of the photo-excited probe in the charge-transfer state [4–7]. Based on comparisons between effects of protic and aprotic solvents, specific solvent interactions (presumably involving hydrogen bonds), also contribute to the solvatochromatism of these probes [8–10]. These strong solvent effects have been used to provide indirect estimations of membrane order and fluidity, which appear to correlate with water invasion into the bilayer [11,12]. Typically, these solvent effects are quantified by calculating a parameter termed "Generalized Polarization" (GP) [4,11] or by deconvolution of spectral components by non-linear regression [13,14]. With these methods, physical phenomena such as lipid phases have been readily observed [4,11,15–18].

Saturated phospholipids display a strong phase transition from a solid ordered phase to a liquid disordered phase (liquid–crystalline or L_α) at temperatures that depend on the length of the chains and the chemical structure of the heads. Although many methods for studying these phases suggest that the liquid disordered phase displays stable properties as temperature is raised beyond the main phase transition, the fluorescence of these naphthalene derivatives suggests otherwise. Studies of either saturated phosphatidylcholine or phosphatidylglycerol consistently show a steady increase of apparent membrane polarity (i.e. decreased GP value or stronger solvent relaxation) as a function of temperature well above the lipid melting point [4,13,19].

The molecular basis for this sensitivity of membrane polarity to high temperatures is not known. Early observations with Laurdan attributed this phenomenon simply to the responsiveness of the probe to dipolar relaxations without further detail [4]. A more specific explanation was

* Corresponding author at: Department of Physiology and Developmental Biology, Brigham Young University, Provo, Utah 84602. Tel.: +1 801 422 2353.
E-mail address: john_bell@byu.edu (J.D. Bell).

http://dx.doi.org/10.1016/j.bbamem.2014.12.021
0005-2736/© 2014 Elsevier B.V. All rights reserved.

offered by investigators studying Laurdan spectra and anisotropy with dilaurylphosphatidylcholine and dipalmitoylphosphatidylglycerol in the liquid disordered state [19]. This explanation argued that changes in the emission spectrum as a function of temperature reflect concomitant increases in the kinetic energy of membrane water molecules facilitating their ability to rotate and therefore respond to the fluorophore's excited state dipole.

We report here a study designed to delineate the mechanism behind the changes in membrane polarity observed in the liquid crystalline state. We have considered the hypothesis proposed above (faster water rotation) as well as an alternative that these effects result instead from increases in the number and/or penetration depth of bilayer water molecules. We take advantage of recent observations from kinetic analyses of probe equilibration suggesting that these naphthalene derivatives may reside in at least two configurations in the membrane and that one can learn additional detail about membrane dynamics by considering the properties of those configurations [20,21]. For such studies, Patman appears ideally suited [20], and we have therefore focused our attention on the behavior of that probe with unilamellar vesicles of various saturated and unsaturated phosphatidylcholines. The results unexpectedly provided evidence that phospholipid behavior is more diverse at temperatures far about the phase transition than previously reported.

2. Materials and methods

All of the experimental methods used in this study have been described in [20]. Lipid stocks (all purchased from Avanti Polar Lipids, Alabaster, AL) were dissolved in chloroform then dried under a nitrogen stream followed by high vacuum. Unilamellar vesicles were prepared by extrusion (100 nm pore size). When high salt concentrations were used (1 or 5 M NaCl, KCl, or $CaCl_2$), vesicles were equilibrated with aqueous solutions of the salt for at least an hour with repeated raising and lowering of temperature through the relevant lipid main phase transition. Steady-state fluorescence with Patman and Laurdan (Molecular Probes; now Life Technologies, Grand Island, NY) was acquired at dual emission wavelengths optimized for separation of nonpolar (short wavelength, 435 nm) and polar (long wavelength, 500 nm) spectral components or as spectra with excitation of 350 nm and a 4 nm excitation and emission bandpass. Suspensions of vesicles in citrate buffer (20 mM Na citrate, 150 mM KCl, pH 7; 50 μM phospholipid) were temperature-equilibrated in the spectrofluorometer for at least 6 min prior to initiating data acquisition. After 100 s, Patman or Laurdan was added (250 nM). When applicable, the value of the spectrum GP was calculated from data at 435 and 500 nm (difference of intensity at 435 and 500 nm divided by the sum of the two as explained) [11,17]. Steady-state anisotropy values were obtained using Glan–Thompson polarizers with corrections for wavelength-dependent differences in polarizer transmission and calculated as described previously for our instrument [17].

3. Calculations

3.1. Monte Carlo simulations

Monte Carlo simulations of spectra involved the following three assumptions:

1. The emission spectrum was assumed to be described approximately by a single normal probability distribution.
2. Water molecules were assumed to relax around the electric field of the excited state as a first-order exponential decay.
3. The emission wavelength for individual probe molecules was assumed to shift toward longer wavelengths directly proportional to the degree to which water molecules have relaxed around the excited state.

Four constants were applied based on observed values: the average excited state lifetime (τ, 3 ns for Patman, [5]), the observed emission maximum for unrelaxed probe (λ_0, 433 nm), the observed emission maximum for fully relaxed probe (λ_R, 480 nm), and the standard deviation for the unrelaxed emission spectrum (σ_λ, 34 nm). The independent variables in the simulations were the probability of water molecules in the vicinity of the probe (P_w) and the rate constant for water relaxation (k_w, ~0.6 ns^{-1}, [5,22]). A total of five random numbers were applied to each probe (R_1... R_5). R_1 was used to determine the energy of fluorescence emission ($1/\lambda$) for each probe molecule by setting it equal to the cumulative probability given by integrating the normal distribution

$$R_1 = \frac{1}{2}\left[1 + \operatorname{erf}\left(\frac{(1/\lambda - 1/\lambda_0)}{\sigma_\lambda\sqrt{2}}\right)\right] \tag{1}$$

where the integration range in the error function was 0 to $1/\lambda$. The unknown, λ, was solved numerically from Eq. (1) by interpolation.

R_2 was used to determine whether a water molecule was present for each probe. Hence, if $R_2 < P_w$, a water molecule was assigned to the probe and allowed to alter the energy of emission so that the final emission wavelength, λ_{em} was greater than λ from Eq. (1). Otherwise, the value of λ from Eq. (1) was retained. For simplicity, each probe with $R_2 < P_w$ was paired with a single water molecule, and changes in emission energy were attributed to the rotational positioning of that single water. This decision to pair the probe with a single water molecule is undoubtedly an oversimplification [23], but it does not interfere with the nature of the simulation results.

For those probes influenced by water in the simulation, R_3 was used to determine t, the time elapsed between probe excitation and emission:

$$t = -\tau \ln(R_3) \tag{2}$$

The starting angle of each water molecule relative to the orientation of its probe partner was determined using R_4. Only the angle between a vector parallel to the excited-state dipole of the probe and one parallel to the permanent dipole of water was considered for determining emission energy. However, since the angle between these dipoles (θ_Z) may be oriented in any direction along the X-Y plane in three-dimensional Euclidean space, the probability of water's orientation relative to the Z axis was weighted by $\sin^2(\theta_Z)$, which generates the following cumulative probability function:

$$R_4 = \frac{1}{\pi}\left[\theta_Z - \frac{1}{2}\sin(2\theta_Z)\right] \tag{3}$$

The value of θ_Z was obtained from R_4 numerically by interpolation using Eq. (3). Lastly, the speed of rotation of each water molecule (r_w) was determined with a fifth random number, R_5, which was set equal to the cumulative distribution function of the classic Maxwell–Boltzmann distribution.

$$R_5 = \operatorname{erf}\left(\frac{r_w}{\sqrt{2}a}\right) - \sqrt{\frac{2}{\pi}\left(\frac{r_w e^{-\left(r_w^2/2a^2\right)}}{a}\right)} \tag{4}$$

where $a = k_w/\sqrt{2}$ and the integration range in the error function was 0 to r_w. The value of r_w was determined from R_5 by interpolation using Eq. (4).

The position of each water molecule at the time of emission was then calculated by combining results from Eqs. 2–4.

$$\theta_{Z,t} = \theta_Z e^{-r_w t} \tag{5}$$

The final step was to calculate the final emission wavelength, λ_{em} for all probes interacting with water (i.e. $R_2 < P_w$).

$$\frac{1}{\lambda_{em}} = \left(\frac{1}{\lambda_R} - \frac{1}{\lambda_0}\right)\cos\theta_{Z,t} + \frac{1}{\lambda} \tag{6}$$

The values of λ_{em} were rounded to the nearest integer for generating the simulated spectra. Each simulation contained 100,000 probe molecules.

3.2. Model for Patman and Laurdan equilibration

Scheme 1 displays the sequential model used to describe the equilibration of Patman or Laurdan with lipid bilayers. For simplicity, it is assumed that when the probe is mixed with an aqueous suspension of phospholipid vesicles, all of the probe molecules immediately adsorb to the membrane surface [20]. Regardless of whether this assumption is valid, we have avoided the issue experimentally by not varying the concentrations of probe and membrane lipid. Hence, Pr_F generically represents probe that has not yet inserted into the bilayer. Secondly, it is assumed that the equilibrium is far in the direction of probe occupying the final state (Pr_R) so that progress toward that state, given by k_0 and k_R, is treated as unidirectional. Pr_0 represents an intermediate state in which probe is inserted into the membrane and therefore removed from the aqueous phase. Whether the rate-limiting step represented by k_0 is the actual insertion of probe into the membrane (which in the case of Laurdan, should be very fast [24]) or is governed by behavior external to the membrane such as low aqueous solubility [6] does not matter in the formalism used here and will be the subject of future studies. Pr_0, however, is not the equilibrium state in this model, and the probe and its interactions with the local microenvironment progress slowly (k_R) to a final relaxed state, Pr_R. The relevant equations describing the process are

$$\frac{dPr_0}{dt} = k_0 Pr_F - k_R Pr_0 \tag{7a}$$

$$\frac{dPr_R}{dt} = k_R Pr_0 \tag{7b}$$

$$Pr_F = Pr_{total} - (Pr_0 + Pr_R) \tag{7c}$$

Substitution and integration yield normalized solutions for P_0 and P_R. (i.e. P_{total} is invariant in experiments and set equal to 1).

$$Pr_0 = \frac{k_0}{k_R - k_0}e^{-k_0 t} + \frac{k_0}{k_0 - k_R}e^{-k_R t} \tag{8a}$$

$$Pr_R = \frac{k_R}{k_0 - k_R}e^{-k_0 t} + \frac{k_R}{k_R - k_0}e^{-k_R t} + 1 \tag{8b}$$

The fluorescence intensities at 435 (F_{435}) and 500 nm (F_{500}) are given by

$$F_{435} = I_0 Pr_0 f_{435,0} + I_R Pr_R f_{435,R} + I_F Pr_F f_{435,F} \tag{9a}$$

$$F_{500} = I_0 Pr_0\left(1 - f_{435,0}\right) + I_R Pr_R\left(1 - f_{435,R}\right) + I_F Pr_F\left(1 - f_{435,F}\right) \tag{9b}$$

$$Pr_F \xrightarrow{k_0} Pr_0 \xrightarrow{k_R} Pr_R$$

Scheme 1. Model for probe equilibration with phospholipid bilayers. Pr_F represents probe not yet inserted into the membrane. Pr_0 is probe at its equilibrium position in the membrane but with the local environment not yet equilibrated with the probe. Pr_R denotes probe in a microenvironment that has relaxed to an equilibrium state.

where I_0, I_R, and I_F are the quantum yields and $f_{435,0}$, $f_{435,R}$, and $f_{435,F}$ are the fraction of the total observed fluorescence emitted at 435 nm for P_0, P_R, and P_F. Based on Eq. 8,

$$F_{435} = Ae^{-k_0 t} + Be^{-k_R t} + C \tag{10a}$$

$$F_{500} = De^{-k_0 t} + Ge^{-k_R t} + H \tag{10b}$$

where A, B, C, D, G, H, k_0, and k_R are obtained by nonlinear regression (Section 3.3), and

$$A = \left(\frac{1}{k_R - k_0}\right)\left[k_0\left(I_0 f_{435,0} - I_F f_{435,F}\right) - k_R\left(I_R f_{435,R} - I_F f_{435,F}\right)\right] \tag{11}$$

$$B = \left(\frac{k_0}{k_R - k_0}\right)\left(-I_0 f_{435,0} + I_R f_{435,R}\right) \tag{12}$$

$$C = I_R f_{435,R} \tag{13}$$

$$D = \left(\frac{1}{k_R - k_0}\right) \times\left[k_0\left(I_0\left(1 - f_{435,0}\right) - I_F\left(1 - f_{435,F}\right)\right) - k_R\left(I_R\left(1 - f_{435,R}\right) - I_F\left(1 - f_{435,F}\right)\right)\right] \tag{14}$$

$$G = \left(\frac{k_0}{k_R - k_0}\right)\left(-I_0\left(1 - f_{435,0}\right) + I_R\left(1 - f_{435,R}\right)\right) \tag{15}$$

$$H = I_R\left(1 - f_{435,R}\right) \tag{16}$$

Rearrangement of Eqs. 11–16 provides explicit solutions for I_0, I_R, $f_{435,0}$, and $f_{435,R}$. None of these solutions requires knowledge of I_F or $f_{435,F}$. Moreover, the observed value of I_F is negligible compared to I_0 and I_R, and it will not be discussed further.

$$I_0 = \frac{k_0(C + H) - (k_R - k_0)(B + G)}{k_0} \tag{17}$$

$$I_R = C + H \tag{18}$$

$$f_{435,0} = \frac{k_0 C - (k_R - k_0)B}{k_0(C + H) - (k_R - k_0)(B + G)} \tag{19}$$

$$f_{435,R} = \frac{C}{C + H} \tag{20}$$

The apparent environmental polarity detected by Patman and Laurdan is frequently expressed as the GP function [4,11]. Values of GP for the initial and relaxed states of the probe are calculated from $f_{435,0}$ and $f_{435,R}$ as follows:

$$GP_0 = 2f_{435,0} - 1 \tag{21a}$$

$$GP_R = 2f_{435,R} - 1 \tag{21b}$$

3.3. Curve fitting

Each pair of probe fluorescence time courses assessed simultaneously at 435 and 500 nm were fit together by nonlinear regression to Eq. 10 with the values of k_0 and k_R constrained to be shared for both wavelengths. Prior to fitting, background intensity (acquired for 100 s with aqueous suspensions of vesicles prior to adding probe) was averaged and subtracted from each data point. I_0, I_R, GP_0, and GP_R were calculated for each time course pair from the values of A, B, C, D, G, H obtained in the regression fits using Eqs. 17–20. In a few cases with Patman, especially at high temperatures, good fits of the data required inclusion of

a third exponential term in Eq. 10. At temperatures greater than 50 °C, the scalar for this third exponential was always positive, and the rate constant was always smaller than the other two. Thus, in those cases, the third exponential represented a slow decline in fluorescence intensity. Control experiments in which the shutter was closed for part of the time course and reopened after several hundred seconds revealed that the slow decline was due to photobleaching, and it was therefore eliminated during the analysis. The same control experiments showed that slow decreases in Laurdan fluorescence intensity were not due to photobleaching, and these were therefore treated as real phenomena associated with equilibration as shown in the text and associated figure at the end of Section 4.

A third exponential was also sometimes observed with Patman at temperatures less than 25 °C. In those cases, the third exponential appeared to represent a splitting of the initial step of probe insertion into the membrane into two components. Accordingly, *A* and *D* were calculated from the sum of the scalars of the two fastest exponential terms, and k_0 was estimated as the average of the rate constants of the same two terms weighted by their respective scalars. Simulated and experimental spectra were fit to the log-normal function as described and recommended previously [14].

4. Results and discussion

4.1. Effects of temperature on membrane polarity and probe anisotropy

Fig. 1 displays GP values for Patman equilibrated with unilamellar vesicles composed of various saturated (Panel A) and unsaturated (Panel B) phosphatidylcholines. In each case, the GP value decreased continuously as a function of temperature above the main transition into the L_α phase. These results are consistent with others reported previously for Laurdan [4,13,17,19], although this may be the first time that it has been shown that the phenomenon occurs even at temperatures more than 90 °C above the melting temperature (open squares in Panel B, dipalmitoleoylphosphatidylcholine melting temperature = −36 °C).

We measured probe anisotropy to consider the possibility that the results in Fig. 1 simply reflect a steady enhancement of membrane disorder or fluidity with increasing temperature. For these measurements, we turned our attention to Laurdan since it would be sensitive to changes in membrane order [17]. Patman was not used for these studies because the anchoring effects of the trimethylammonium group and the longer acyl chain blunt the sensitivity of anisotropy measurements to membrane dynamics [20]. As shown in Fig. 2A, measurements of Laurdan anisotropy (open circles, dashed curve) assessed simultaneously with GP (solid circles and curve) revealed that probe motion was less affected by temperature in the L_α phase than was the environmental polarity around the probe (indicated by GP). The anisotropy trend relative to the change at the phase transition (0.03) was 1/5 of that observed with GP (0.17). These anisotropy measurements were acquired at 435 nm, which may underestimate the actual mobility of Laurdan as suggested by a recent study [19]. We therefore compared anisotropy measurements at 480 nm (Fig. 2B, triangles), as recommended by that study, to those at 435 nm (Fig. 2B, circles). Analysis of the trends demonstrated that the difference in temperature dependence for anisotropy and GP was not an artifact of choice of emission wavelength for the observations (see figure legend for statistics). In summary, relative to the changes associated with lipid melting, Laurdan motion detected by anisotropy was less sensitive to temperature in the L_α phase than was GP. We therefore concluded from these experiments that the changes in GP in the L_α phase were not simply a reflection of general increases in bilayer disorder or fluidity.

4.2. Effects of salts

To verify that water molecules were responsible for the effects of high temperature on GP, the experiments of Figs. 1 and 2A were repeated in the presence of 1 M NaCl. This concentration was chosen to maximize

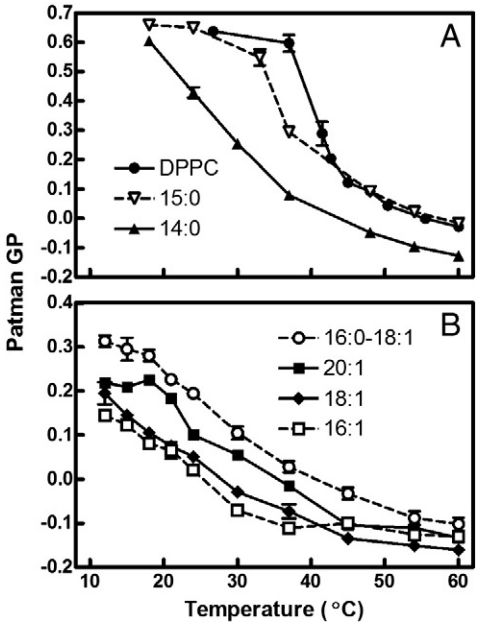

Fig. 1. Effects of temperature on Patman GP values for various phosphatidylcholine vesicles in the L_α phase. Lipids used were all 1,2-diacyl-*sn*-glycero-3-phosphocholines with the following pairs of acyl chains (with melting temperature defined as per the supplier). Panel A: (solid circles) dipalmitoyl (DPPC, 41 °C), (open inverted triangles) dipentadecanoyl (15:0, 35 °C), (solid triangles) dimyristoyl (14:0, 24 °C). Panel B: (open circles) 1-palmitoyl-2-oleoyl (16:0–18:1, −2 °C), (solid squares) dieicosenoyl (20:1 (Cis), −4 °C), (solid diamonds) dioleoyl (18:1 (Δ9-Cis), −17 °C), and (open squares) dipalmitoleoyl (16:1 (Δ9-Cis), −36 °C). Error bars represent SE when applicable (or range when n = 2), n = 1–5. In some cases, the error range was smaller than the diameter of the data point.

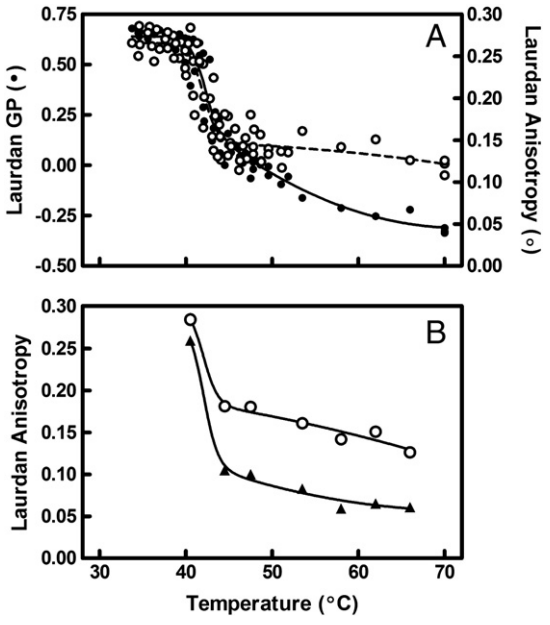

Fig. 2. Comparison of the effects of temperature on Laurdan GP and anisotropy in DPPC vesicles. Panel A: GP (solid circles and curve) and anisotropy values (open circles, dashed curve) were acquired simultaneously. Anisotropy was assessed at 435 nm. Data were scaled in the graph so that the relative magnitudes of decline in GP and anisotropy at the main phase transition coincided. Panel B: Anisotropy values were acquired at both 435 (circles) and 480 nm (triangles) for comparison. The confidence intervals for the slopes of the linear portion of the curves were virtually confluent (−0.0036 to −0.0014 GP units·°C^{-1} at 435 nm; −0.0034 to −0.0011 GP units·°C^{-1} at 480 nm). Data points in both panels represent individual trials. The curves have no theoretical significance.

effects of the salt on the relative water permittivity while minimizing direct effects on the membrane. In bulk solution, 1 M NaCl reduces water permittivity by about 14%, and at the membrane surface, the effect is reported to be even larger (22% reduction) [25,26]. This reduction would be expected to attenuate the solvent relaxation effect by more than 0.1 GP units depending on the distance between responsible waters and the depth of penetration of the salt. Fig. 3A illustrates the effects of NaCl (open triangles) on the temperature dependence of Patman GP with dipalmitoylphosphatidylcholine (DPPC) vesicles. The salt caused a very small elevation of GP at temperatures corresponding to the L_α phase. If the effect on the L_α phase is a reflection of water permittivity, it should have greater impact on Laurdan, which resides more superficially in the membrane and therefore closer to where ions would exert their effect on water. As revealed by Fig. 3B, such was in fact the case. Results qualitatively similar to those shown in Fig. 3A were obtained for both NaCl and KCl, but the effects of these salts on the L_α phase well separated from the melting temperature (70 °C) were about ten times greater with Laurdan than with Patman. To insure that the effects

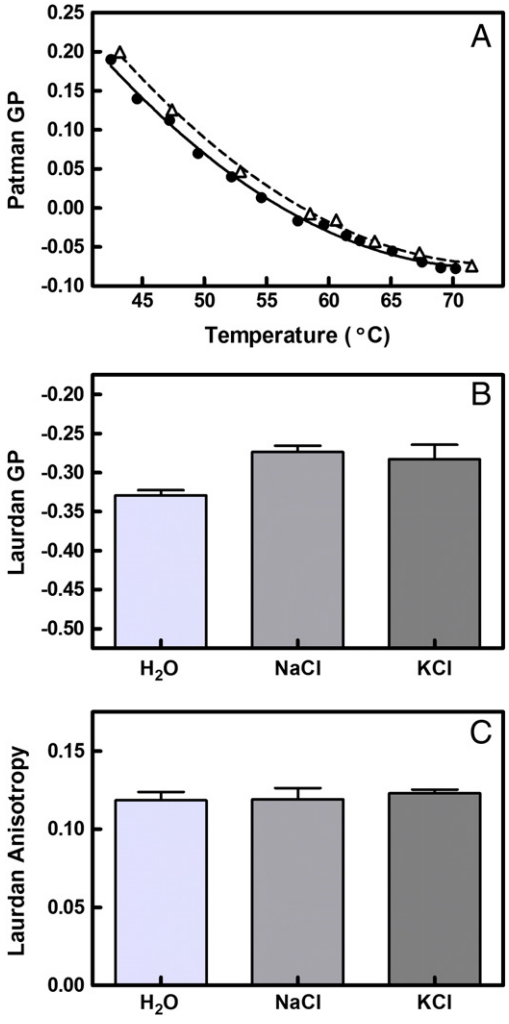

Fig. 3. Effects of salts on GP and anisotropy values. Panel A: The experiment of Fig. 1 (Patman, DPPC) was repeated with vesicles equilibrated with (triangles, dotted curve) or without (circles, solid curve) 1 M NaCl (see Section 2). The curves have no theoretical significance. Panel B: The experiment of Panel A was repeated with vesicles equilibrated with Laurdan and 1 M NaCl, 1 M KCl, or water. Bars are means ± SE of data acquired at temperature = 70 °C, n = 3–4 independent samples. The NaCl and KCl groups were both statistically different from the control (water) by one-way ANOVA followed by a Dunnett's multiple comparison posttest ($p < 0.05$). The spans of the ordinate scales of panels A and B are identical to facilitate comparison. Panel C: Laurdan anisotropy measurements were acquired simultaneously with those shown in panel B. No statistical differences were identified comparing samples with salts to the controls ($p = 0.8$ by one-way ANOVA).

of these ions were not to alter membrane fluidity or order through direct interactions (which are known to occur at higher concentrations as verified by control experiments [27]), we compared the effects of these ions on Laurdan anisotropy and found that there was no difference (Fig. 3C). Based on the overall results in Fig. 3, we concluded that the changes in GP at high temperature are due to water relaxation as has been surmised previously for temperatures near the phase transition [5,11,12,28].

4.3. Monte Carlo simulations of spectra

It has been proposed that the temperature sensitivity of probe GP with lipids in the L_α phase is due to increases in water mobility in the membrane [19]. We reasoned that changes in the rate of water movement versus the number of proximal water molecules would be distinguishable based on emission spectra. To test that idea, we performed Monte Carlo simulations of Patman emission spectra using known values for the probe's fluorescence lifetime with lipids in the L_α phase, reported rates of spectral shifts during water relaxation, and known values for Patman spectral maxima in the unrelaxed and relaxed states (see Section 3.1 and [5,22]). Fig. 4A displays the family of spectra expected as a function of temperature if differences reflect changes in the rate of water relaxation. Fig. 4B illustrates the effect of incremental amounts of water proximal to the probe. In both cases, the data were fit using log-normal functions as described previously [14], and the component spectral elements are plotted in Fig. 4C and D. In the case of spectral shifts caused by incremental increases in water relaxation rate, the spectrum shifts continuously from one extreme to the other (Fig. 4C). However, when the mechanism reflects changes in the amount of proximal water, two spectral components are present, and elevation of temperature alters the relative contribution of each with limited changes in wavelength maxima (Fig. 4D). As shown in Fig. 4E–H, the experimental spectral changes observed with Patman (Panels E and F) as well as Laurdan (Panels G and H; see also [14]) match the simulations in Fig. 4B and D. We therefore concluded that the effect of temperature on bilayer properties in the L_α phase is mostly a result of water access to the membrane rather than water mobility. In drawing that conclusion, we recognize that the rate of water movement in the membrane surely increases with temperature; in fact, evidence from Patman lifetime measurements verifies that such is the case [5,22]. The point of the simulations, which used authentic values for parameters such as solvent relaxation rates, is that even at the lowest temperatures studied, the rate of water movement in the L_α phase is already sufficiently fast that it is not rate-limiting for the observed spectral changes. Further increases in water movement rate, then, at higher temperatures do not impact the spectrum.

4.4. Patman equilibration kinetics

Previously, it was shown that additional detail about membrane and water dynamics could be learned by examining the kinetics of Patman equilibration with the membrane at two emission wavelengths corresponding to nonpolar and polar environments of the probe [20]. As illustrated in Fig. 5, the time courses of Patman equilibration at 435 (blue curves) and 500 nm (green curves) were complex (involving more than one rate and therefore double-exponential as in Eq. 10. The solid curves denote fits of the data to Eq. 10, and the dashed curves are fits to a single-exponential version of Eq. 10. This complexity in the time courses results in GP values that also show a multi-faceted time profile; in some cases, a rapid rise is followed by a decline, and in other cases, by a slow elevation in GP (red curves, Fig. 5). These data imply that more than one process is involved in the equilibration of the probe with the membrane, and the simplest explanation for that complexity is a sequential model of probe insertion into the membrane followed by a secondary process in which the local environment (membrane, probe, and associated waters) relaxes (Scheme 1; see derivation in Section 3.2). Analysis of time courses such as those

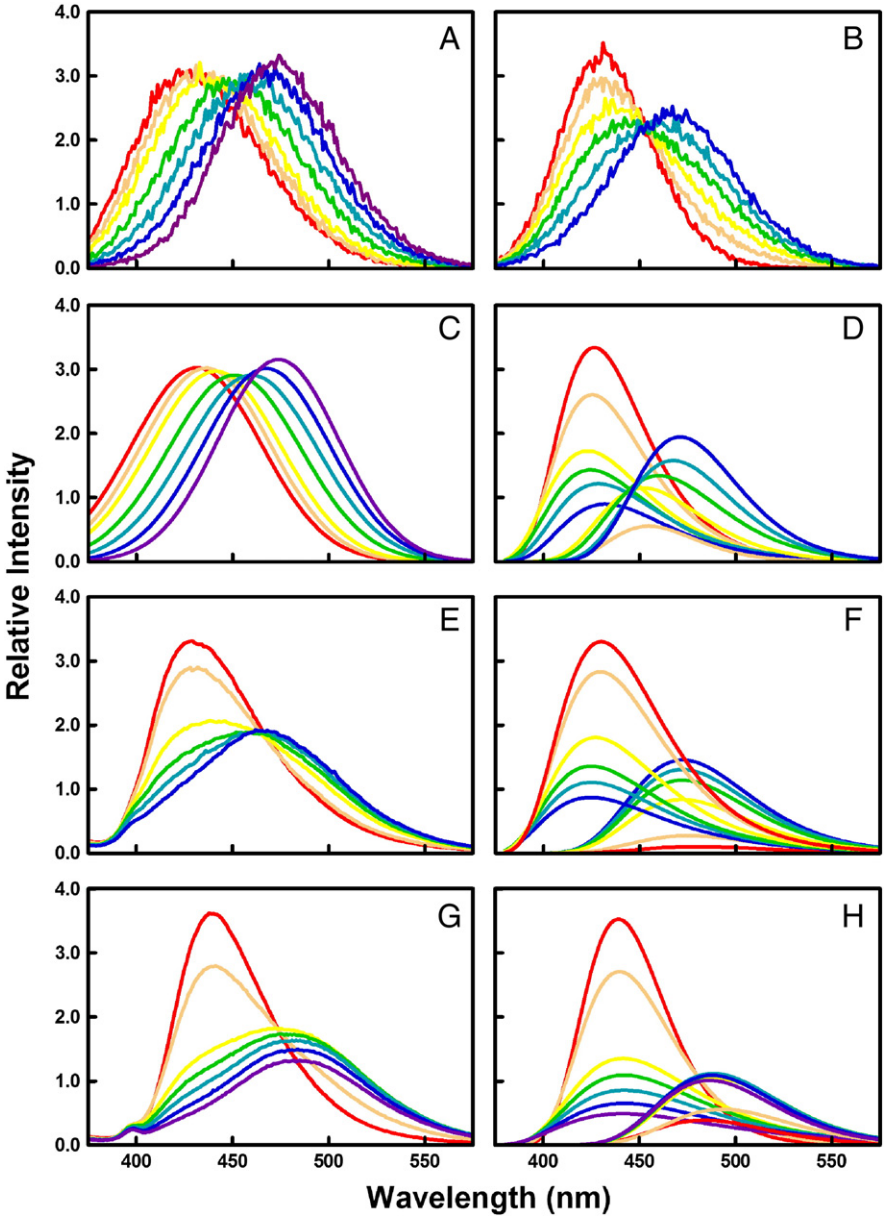

Fig. 4. Monte Carlo simulations of hypothetical effects of bilayer water on Patman spectra compared to experimental data. Panel A: Patman emission spectra were simulated as explained in Section 3.1 with $P_w = 1$ and $k_w = \sim 0, 0.02, 0.04, 0.1, 0.2, 0.4, 1.0\ ns^{-1}$ (left to right spectra). Panel B: The simulations of panel A were repeated with $k_w = 0.4\ ns^{-1}$ and Pw = 0, 0.2, 0.4, 0.6, 0.8, 1.0 (upper left to lower left). Panels C and D: Spectral components of panels A (C) and B (D) were obtained as explained in Section 3.3. Panel E: Emission spectra of Patman were obtained on a pre-equilibrated sample at 27, 38, 41, 43, 47, 55 °C (upper left to lower left), and its spectral components are shown in panel F. Panel G: Emission spectra of Laurdan were obtained on a pre-equilibrated sample at 30, 41, 46, 50, 56, 63, and 70 °C (upper left to lower left), and the spectral components are shown in Panel H.

shown in Fig. 5 generates six parameter values: the rate of initial interaction of the probe with the membrane (k_0), the rate of subsequent relaxation of the local probe environment (k_R), probe emission intensity initially and after relaxation (I_0 and I_R), and the apparent polarity of the local probe environment initially and after relaxation expressed as GP values (GP_0 and GP_R). For ease of presentation during the next few paragraphs, we will assume that this model is applicable, and we will discuss alternative interpretations thereafter.

This approach allowed us to address two questions: 1) is the decremental change in GP with temperature an artifact of slow membrane perturbation by the probe? 2) Is the response of the membrane to insertion of the probe uniform across temperature in the L_α phase? Fig. 6A displays the value of GP detected by Patman with dioleoylphosphatidylcholine vesicles immediately after entering the bilayer prior to membrane responses to its presence (GP_0). Similar results were obtained with all the lipids included in Fig. 1 (not shown). These data answered the first question conclusively; the lowering of GP by elevated temperature with phospholipids in the L_α phase is not caused by slow effects of the probe on the membrane. The second question was addressed by considering the change in Patman GP (GP_0 to GP_R, illustrated by red curves in Fig. 5) during membrane relaxation as a function of temperature (Fig. 6B, DPPC). Surprisingly, the effect of temperature on ΔGP with DPPC vesicles was complex. For temperatures within the first 10 °C above the lipid phase transition, GP was lowered as the membrane responded to insertion of Patman. At higher temperatures, the opposite effect was observed. Clearly, these observations provide a definitive "no" to the second question and also indicate that complex membrane dynamics responding to a contaminating molecule depend on temperature in an intriguing and multidimensional manner. Analogous responses were observed with other saturated and unsaturated phosphatidylcholines with one additional feature (Fig. 6C–H). For lipids with melting temperatures between −4 and 33 °C (Panels C–F), GP increased after probe insertion at

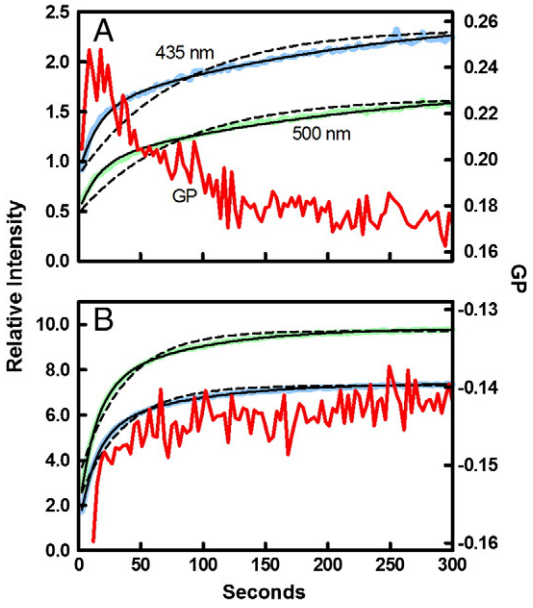

Fig. 5. Time profiles of Patman equilibration with dioleoylphosphatidylcholine (18:1 (Δ9-Cis)) vesicles. Equilibration was observed simultaneously at 435 (blue curves) and 500 nm (green curves) at 15 (A) and 45 °C (B). Curves were fit to both double exponential (solid black curves) and single exponential (dashed curves) versions of Eq. 10. Corresponding GP values are shown in red.

temperatures closest to the melting point. Over the next several degrees, the change in GP became smaller, and in most cases was negative as observed for DPPC. The increase in ΔGP to positive values at the highest temperatures seen with DPPC was universal among the lipids tested. Assuming that the two lowest-melting lipids, dioleoyl- (−17 °C, Panel G) and dipalmitoleoylphosphatidylcholine (−36 °C, Panel H), exhibited similar behavior, it appeared that the temperature range studied represented the upper half of this profile for those lipids. Hence, for each lipid, there was a minimum in ΔGP. When the temperature corresponding to that minimum was compared to the melting temperature, a linear relationship with a strong correlation was observed (slope = 0.44 ± 0.10, $r^2 = 0.87$, $p = 0.02$, n = 5).

The data of Fig. 5 suggested that the overall intensity of Patman emission continued to increase after probe insertion. In fact, analysis of the change in intensity after relaxation ($I_R - I_0$) demonstrated that such was universal among all the lipids tested. Moreover, the magnitude of this change was invariant with temperature and lipid type ($p > 0.05$ in each case by ANOVA, n = 7–10 temperatures and 1–4 replicates at each temperature per lipid type). In contrast, the value of I_0 did increase with temperature linearly in the L_α phase up to about 45 °C, probably representing greater ease of probe insertion. Above that point, I_0 was independent of temperature. Together, these results suggested that part of the relaxation process is to rid Patman molecules of associated quenchers, presumably waters. The lack of lipid dependence and freedom from the complications observed for membrane polarity in Fig. 6 argue that these effects on emission intensity involve only the general transfer of Patman from an aqueous to hydrophobic environment and not on structural details of the lipids. The more intriguing observation was the slowness of this secondary process of intensity increasing from I_0 to I_R; half-times ranged from about 350 to 14 s as temperature increased from 12 to 60 °C. In the absence of a better understanding of the mechanisms involved in solvent quenching of naphthalene fluorescence, we are unable to draw a definitive conclusion for the details of this event, but one possibility is that water molecules hydrogen-bonded to the carbonyl group of Patman dissociate slowly upon transfer of the molecule into the bilayer [20].

In summary, the kinetic observations with Patman present a scenario in which the probe appears to enter the membrane on a time scale of seconds (half-times ranging from 35 to <2 s depending on temperature) followed by a secondary event that occurs at 1/10 of that rate and involves both an additional increase in emission intensity and a change in the local membrane polarity of either positive or negative direction depending on the temperature relative to the melting point of the lipid. This complexity of these membrane polarity changes suggests the participation of at least three processes. We propose that these processes are 1) a foundational ordering effect of inserting a probe with a saturated acyl tail and a positive charge into a fluid membrane, 2) a counter-balancing entropic effect that emerges as temperature is raised, and 3) another entropic effect that alters vertical probe distribution in the membrane. This proposal is described by the following narrative. First, the local ordering effect of probe insertion reduces the availability of water molecules to participate in solvent relaxation and therefore produces the increase in GP upon probe insertion observed for most lipids at temperatures just above the melting point. Perhaps the structural matching of the Patman and DPPC tails accounts for the absence of this effect in that particular case (Fig. 6B). Second, since this local ordering effect would involve enthalpy changes (due to interactions among phospholipid and Patman tails and possible electrostatic interactions between the trimethylammonium of Patman and phospholipid phosphates), it would be unable to compensate for the entropically-driven disordering effects of elevated temperature. Hence, the positive increase in GP is reduced and even becomes negative as temperature is increased. The negative component could indicate that structural mismatches in the head group region between the probe and the surrounding phospholipids creates spaces for additional water invasion that become available once the ordering effect of the probe is eliminated by increased temperature. Third, we postulate that increases in temperature also affect the diversity of vertical positioning of Patman in the membrane. It has already been shown experimentally that Patman displays a range of vertical locations in the bilayer [29]. It makes sense that this range would broaden as temperature is increased due to entropic considerations. Since Patman's average location in the membrane is sufficiently close to bilayer waters for the solvent relaxation effect to be manifest, a symmetrical broadening of its vertical distribution would increase the proportion of Patman molecules distanced from water's influence (those at the superficial end of the distribution would not be changed since they are already in juxtaposition to water). Thus, the net effect of that broadening would be an increase in GP, which is what dominates experimentally at the highest temperatures. This narrative certainly cannot be proven with the existing data, but it provides a reasonable hypothesis as a basis for future structural investigations into the equilibrium disposition of Patman in a fluid membrane far from the melting point.

We have presented this part of the study assuming that the model shown in Scheme 1 is true for Patman. An alternative explanation for the dual-rate equilibration time courses shown in Fig. 5 has been proposed previously [20]. In that former model, the two rates represented parallel paths to two different configurations of the probe. We focused here on the sequential model of Scheme 1 simply because it is more parsimonious in terms of the number of parameters involved. Nonetheless, it may be more palatable to imagine a scenario in which most of the probe molecules insert relatively quickly into one configuration while a few insert more slowly (perhaps impaired by those already present in the membrane or perhaps involving aggregation of probe molecules) into a slightly different micro-environment. If this alternative model is true, however, there should be support from structural or theoretical studies for two configurations of Patman at equilibrium. To date, no such supporting evidence exists, although the relevant studies so far have involved only Laurdan and Prodan [9]. Thus, on the one hand, structural studies with Patman are needed, both experimental and theoretical, and we are currently involved in such efforts. On the other hand, reliance on evidence with Laurdan is not unreasonable since Laurdan also showed a two-phase equilibration process (Fig. 7A). Interestingly, there were quantitative differences between results with

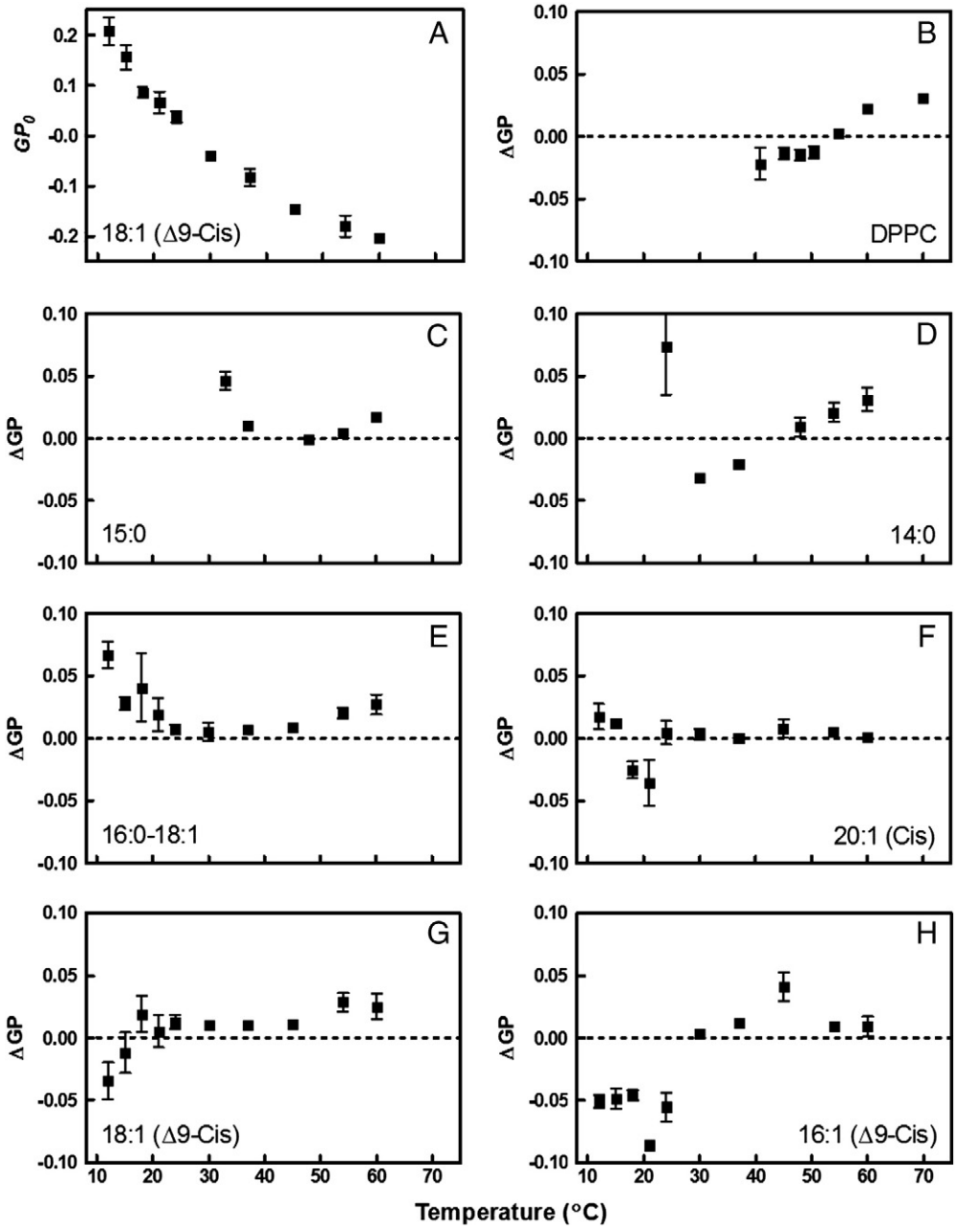

Fig. 6. Changes in Patman GP observed during equilibration from initial to relaxed state. Data such as shown in Fig. 5 were analyzed as described in Section 3.3. Panel A: values of GP_0 from that analysis (18:1 (Δ9-Cis)). Differences in GP during relaxation ($GP_R - GP_0$) were calculated for (B) DPPC, (C) dipentadecanoyl (15:0), (D) dimyristoyl (14:0), (E) 1-palmitoyl-2-oleoyl (16:0–18:1), (F) dieicosenoyl (20:1 (Cis)), (G) dioleoyl (18:1 (Δ9-Cis)), and (H) dipalmitoleoyl (16:1 (Δ9-Cis)). Data points represent 1 to 4 independent samples (error bars represent SE).

Laurdan compared to Patman. First, the intensity decreased during the slow phase of Laurdan equilibration (Fig. 7B, squares, solid lines) rather than increasing as it did with Patman. Second, although the environmental polarity during the slow phase followed a pattern similar to Patman (compare triangles and dashed lines in Fig. 7B to Fig. 6B), the changes in GP values were never positive like they sometimes were with Patman. These observations merit further investigation in the future, but at a minimum, they suggest that the longer tail and positive charge of Patman are relevant to the observed kinetics. After considering all these issues, we tentatively propose the sequential model in Scheme 1 for equilibration of these probes in the membrane, assuming that future investigations will elucidate the matter. Regardless of these details, the observation remains that membrane dynamics in response to and detected by these probes are not uniform as a function of temperature in the L_α phase.

5. Conclusions

The data of this study have enabled us to draw four conclusions about the behavior of the L_α phase at temperatures extending far (at least 90 °C) beyond the phospholipid melting point. 1) As detected by both Patman and Laurdan, the apparent polarity of the bilayer continuously increases. 2) This effect represents interactions of water molecules with the probe and does not coincide with a proportional increase in probe mobility. 3) The increased polarity represents an elevation in access to water molecules rather than increased mobility of existing bilayer waters. This conclusion may relate to a recent assertion from computer simulations that waters responsible for solvent relaxation effects on Laurdan are hydrogen-bonded to phospholipid carbonyl groups and therefore not freely-rotating as implied in earlier studies [23]. 4) The observed increase in polarity is not an artifact from probe

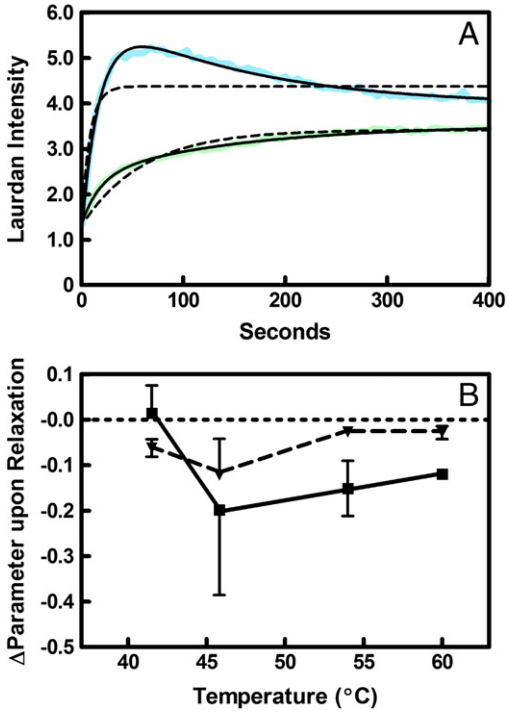

Fig. 7. Laurdan equilibration parameters. Panel A: Laurdan equilibration was observed simultaneously at 435 (blue curves) and 500 nm (green curves) at 45 °C. Curves were fit to both double exponential (solid black curves) and single exponential (dashed curves) versions of Eq. 10. Panel B: Differences in parameter values upon relaxation (squares: $I_R - I_0$, normalized to I_R; triangles: $GP_R - GP_0$) were calculated as explained in Section 3.2.

perturbation of the membrane as revealed by the kinetics of probe equilibration with the bilayer. The equilibration of Patman with the membrane involves at least two steps (or configurations). These steps (or configurations) can be distinguished by the membrane microenvironment reported by the probe. The difference in those microenvironments also changes with temperature in the L_α phase in that the relaxed environment is less polar than the initial environment detected by Patman at temperatures near the melting point, more polar at higher temperatures, and again less polar as temperature is raised further. Laurdan also encounters this level of complexity as it equilibrates, although the relationship to temperature differs quantitatively from that experienced by Patman. Based on computer simulations, these equilibration steps probably reflect local environmental responses to the presence of the probe instead of probe migrating into its final location, which should occur on the nanosecond rather than second time scale [24].

We think the kinetic approach described here is significant for three reasons. First, it provides a novel way to address and deal quantitatively with potential artifacts of these fluorescent probes as membrane contaminants. More importantly, when complemented with structural studies at equilibrium, it is a potential means for understanding in molecular detail basic principles of what happens to the membrane environment around an individual amphipathic molecule as it penetrates the membrane. Third, it provides evidence of unexpected and interesting membrane behaviors far from the phase transition. This latter observation may have relevance to cell membranes which are naturally in that condition of being far removed from a phase transition.

References

[1] G. Weber, F.J. Farris, Synthesis and spectral properties of a hydrophobic fluorescent probe: 6- propionyl-2-(dimethylamino)naphthalene, Biochemistry 18 (1979) 3075–3078.
[2] J.R. Lakowicz, D.R. Bevan, B.P. Maliwal, H. Cherek, A. Balter, Synthesis and characterization of a fluorescence probe of the phase transition and dynamic properties of membranes, Biochemistry 22 (1983) 5714–5722.
[3] T. Parasassi, F. Conti, E. Gratton, Time-resolved fluorescence emission spectra of Laurdan in phospholipid vesicles by multifrequency phase and modulation fluorometry, Cell. Mol. Biol. 32 (1986) 103–108.
[4] T. Parasassi, G. De Stasio, A. d'Ubaldo, E. Gratton, Phase fluctuation in phospholipid membranes revealed by Laurdan fluorescence, Biophys. J. 57 (1990) 1179–1186.
[5] J.R. Lakowicz, G. Laczko, H. Cherek, E. Gratton, M. Limkeman, Analysis of fluorescence decay kinetics from variable-frequency phase shift and modulation data, Biophys. J. 46 (1984) 463–477.
[6] T. Parasassi, E.K. Krasnowska, L. Bagatolli, E. Gratton, LAURDAN and PRODAN as polarity-sensitive fluorescent membrane probes, J. Fluoresc. 8 (1998) 365–373.
[7] M. Viard, J. Gallay, M. Vincent, O. Meyer, B. Robert, M. Paternostre, Laurdan solvatochromism: solvent dielectric relaxation and intramolecular excited-state reaction, Biophys. J. 73 (1997) 2221–2234.
[8] M. Bacalum, B. Zorila, M. Radu, A. Popescu, Laurdan solvatochromism: influence of solvent polarity and hydrogen bonds, Optoelectron. Adv. Mater. 7 (2013) 456–460.
[9] G. Parisio, A. Marini, A. Biancardi, A. Ferrarini, B. Mennucci, Polarity-sensitive fluorescent probes in lipid bilayers: bridging spectroscopic behavior and microenvironment properties, J. Phys. Chem. B 115 (2011) 9980–9989.
[10] A. Marini, A. Munoz-Losa, A. Biancardi, B. Mennucci, What is Solvatochromism? J. Phys. Chem. B 114 (2010) 17128–17135.
[11] T. Parasassi, G. De Stasio, G. Ravagnan, R.M. Rusch, E. Gratton, Quantitation of lipid phases in phospholipid vesicles by the generalized polarization of Laurdan fluorescence, Biophys. J. 60 (1991) 179–189.
[12] T. Parasassi, M. Di Stefano, M. Loiero, G. Ravagnan, E. Gratton, Cholesterol modifies water concentration and dynamics in phospholipid bilayers: a fluorescence study using Laurdan probe, Biophys. J. 66 (1994) 763–768.
[13] A.D. Lucio, C.C. Vequi-Suplicy, R.M. Fernandez, M.T. Lamy, Laurdan spectrum decomposition as a tool for the analysis of surface bilayer structure and polarity: a study with DMPG, peptides and cholesterol, J. Fluoresc. 20 (2010) 473–482.
[14] M. Bacalum, B. Zorila, M. Radu, Fluorescence spectra decomposition by asymmetric functions: Laurdan spectrum revisited, Anal. Biochem. 440 (2013) 123–129.
[15] T. Parasassi, G. Ravagnan, R.M. Rusch, E. Gratton, Modulation and dynamics of phase properties in phospholipid mixtures detected by Laurdan fluorescence, Photochem. Photobiol. 57 (1993) 403–410.
[16] T. Parasassi, M. Di Stefano, M. Loiero, G. Ravagnan, E. Gratton, Influence of cholesterol on phospholipid bilayers phase domains as detected by Laurdan fluorescence, Biophys. J. 66 (1994) 120–132.
[17] F.M. Harris, K.B. Best, J.D. Bell, Use of laurdan fluorescence intensity and polarization to distinguish between changes in membrane fluidity and phospholipid order, Biochim. Biophys. Acta 1565 (2002) 123–128.
[18] B.M. Stott, M.P. Vu, C.O. McLemore, M.S. Lund, E. Gibbons, T.J. Brueseke, H.A. Wilson-Ashworth, J.D. Bell, Use of fluorescence to determine the effects of cholesterol on lipid behavior in sphingomyelin liposomes and erythrocyte membranes, J. Lipid Res. 49 (2008) 1202–1215.
[19] C.C. De Vequi-Suplicy, C.R. Benatti, M.T. Lamy, Laurdan in fluid bilayers: position and structural sensitivity, J. Fluoresc. 16 (2006) 431–439.
[20] H. Franchino, E. Stevens, J. Nelson, T.A. Bell, J.D. Bell, Wavelength dependence of Patman equilibration dynamics in phosphatidylcholine bilayers, Biochim. Biophys. Acta 1828 (2013) 877–886.
[21] E. Gibbons, K.R. Pickett, M.C. Streeter, A.O. Warcup, J. Nelson, A.M. Judd, J.D. Bell, Molecular details of membrane fluidity changes during apoptosis and relationship to phospholipase A(2) activity, Biochim. Biophys. Acta 1828 (2013) 887–895.
[22] A. Olzynska, A. Zan, P. Jurkiewicz, J. Sykora, G. Grobner, M. Langner, M. Hof, Molecular interpretation of fluorescence solvent relaxation of Patman and 2H NMR experiments in phosphatidylcholine bilayers, Chem. Phys. Lipids 147 (2007) 69–77.
[23] P. Jurkiewicz, L. Cwiklik, P. Jungwirth, M. Hof, Lipid hydration and mobility: an interplay between fluorescence solvent relaxation experiments and molecular dynamics simulations, Biochimie 94 (2012) 26–32.
[24] J. Barucha-Kraszewska, S. Kraszewski, P. Jurkiewicz, C. Ramseyer, M. Hof, Numerical studies of the membrane fluorescent dyes dynamics in ground and excited states, Biochim. Biophys. Acta 1798 (2010) 1724–1734.
[25] J.B. Hasted, D.M. Ritson, C.H. Collie, Dielectric properties of aqueous ionic solutions.1.2, J. Chem. Phys. 16 (1948) 1–21.
[26] J.G. Lessard, M. Fragata, Micropolarities of lipid bilayers and micelles.3. Effect of mono-valent ions on the dielectric-constant of the water membrane interface of unilamellar phosphatidylcholine vesicles, J. Phys. Chem. 90 (1986) 811–817.
[27] G. Pabst, A. Hodzic, J. Strancar, S. Danner, M. Rappolt, P. Laggner, Rigidification of neutral lipid bilayers in the presence of salts, Biophys. J. 93 (2007) 2688–2696.
[28] J.B. Henshaw, C.A. Olsen, A.R. Farnbach, K.H. Nielson, J.D. Bell, Definition of the specific roles of lysolecithin and palmitic acid in altering the susceptibility of dipalmitoylphosphatidylcholine bilayers to phospholipase A2, Biochemistry 37 (1998) 10709–10721.
[29] P. Jurkiewicz, A. Olzynska, M. Langner, M. Hof, Headgroup hydration and mobility of DOTAP/DOPC bilayers: a fluorescence solvent relaxation study, Langmuir 22 (2006) 8741–8749.